16th World Conference on Earthquake, 16WCEE 2017

Santiago Chile, January 9th to 13th 2017

Paper N° 472 (Abstract ID)

Registration Code: S-XXXXXXXX

STRUCTURAL PERFORMANCE EVALUATION OF R/C EXTERIOR/PARTITION FLAT WALLS MONOLITHICALLY CONSTRUCTED IN MOMENT RESISTING FRAMES

Y. Sanada[(1)], Y. OJIO[(2)], T. AKAHORI[(3)] Y. KIM[(4)]

[(1)] *Associate Professor, Osaka University, sanada@arch.eng.osaka-u.ac.jp*
[(2)] *Former Graduate Student, Osaka University, ojio.yuto@gmail.com*
[(3)] *Former Graduate Student, Osaka University, takumiakahori@gmail.com*
[(4)] *Assistant Professor, Hongik University, yskim1220@gmail.com*
…

Abstract

Exterior/partition flat walls monolithically constructed in concrete buildings were severely damaged by the 2011 earthquake off the Pacific coast of Tohoku, Japan. Damage to exterior/partition flat walls significantly prevented concrete buildings from immediate occupancy. Although this type of wall is commonly regarded as non-structural wall, it seems to potentially affect the seismic performance and behavior of overall buildings because of its monolithic connection to structural components. Therefore, this paper investigates fundamental behavior and performance of a typical flat wall through experimental and analytical approaches.

This paper focuses on a steel reinforced concrete (SRC) residential building that was damaged by the 2011 earthquake off the Pacific coast of Tohoku. Exterior flat walls with the width of approximately 1 m were monolithically connected to structural beams and significantly damaged during the earthquake. A 1/2.5 scale one-bay frame model partially representing the 10th story of the building was designed, fabricated, and tested under static cyclic loads. Contributions of the flat wall to the overall performance/behavior were obtained by measuring shear and axial forces of each column.

A beam yielding mechanism was formed in the overall specimen with a shear failure of the flat wall. The specimen deteriorated with buckling of beam longitudinal rebars. The maximum shear force of 87 kN, which corresponded to approximately one-third of the overall strength, was sustained by the flat wall until the shear failure, which means that this type of wall is not necessarily negligible for the seismic performance/behavior of buildings at design drift levels. Such high contribution of the flat wall attributed a passive compression caused by its nonlinear axial elongation. On the other hand, the resistance was completely lost after the shear failure.

Experimental results were simulated by numerical analyses using several macro models. In particular, the flat wall was replaced by three types of macro models: Case 1a, Case 1b, and Case 2. Multi Spring (MS) model was used for Case 1a and Case 1b. Shear strength deterioration was considered only for Case 1b. On the other hand, Isoparametric Element (IPE) model was used for Case 2 which considered the axial-flexural-shear behavior interactions. Consequently, Case 1b and Case 2 successfully simulated the experimental lateral force-story drift angle relationship for the overall specimen as well as flat wall. Shear strength drop of the flat wall was represented except for Case 1a. However, only Case 2 could evaluate the loss of axial resistance with shear failure of the flat wall, because the axial-flexural-shear behavior interactions were considered only for the model.

Keywords: nonstructural wall; reinforced concrete; seismic performance

1. Introduction

Reinforced concrete (R/C) exterior/partition flat walls in concrete buildings, which were commonly designed as nonstructural walls in Japan, were severely damaged by the 2011 earthquake off the Pacific coast of Tohoku [1]. Such damage was observed to monolithic nonstructural walls in relatively old buildings, because seismic slits, which prevent damage to the nonstructural walls by isolated from structural components, had been widely applied to recent concrete buildings in Japan after the 1995 Kobe earthquake [2]. The old-fashioned nonstructural walls had limited ductility; therefore, when they responded beyond the deformation capacities with large story drifts of ductile moment-resisting frames, severe damage occurred due to the monolithic construction. It was revealed that the concrete buildings lost their functions due to failure of the nonstructural walls even though the structural components were not significantly damaged.

Earthquake-damaged R/C buildings are generally judged to be restored/demolished according to the guidelines for post-earthquake damage evaluation [3] in Japan. The guidelines provide a method to evaluate the residual ultimate seismic performance of the earthquake-damaged R/C buildings, by which the buildings are classified into six damage ratings: no, slight, light, moderate, and heavy damage and collapse. Comparing the resultant damage rating of an earthquake-damaged building of interest with an intensity of ground motions on-site, an action of restoration or demolition is suggested for the building. After the 2011 Tohoku earthquake, however, several specific problems were pointed out when it was applied to ductile concrete buildings with damage to R/C nonstructural flat walls, because the structural performance of such walls was not clear.

Therefore, the objectives of this study are to experimentally clarify the structural performance of a typical R/C nonstructural flat wall considering complex interactions with structural components, and to provide an appropriate numerical model for R/C nonstructural walls.

2. Organization Earthquake-Damaged Building with Nonstructural Wall Failure

2.1 Summary of investigated building

This study focuses on an 11-story steel reinforced concrete (SRC) residential building in Sendai city, which was damaged by the 2011 earthquake off the Pacific coast of Tohoku, as shown in Fig. 1. Figure 2 presents the ground floor plan. The building had an approximately symmetric regular plan with the dimensions of 71 m in the longitudinal direction and 27 m in the transverse direction, respectively. The structural systems in the longitudinal and transverse directions were SRC moment-resisting frames without and with structural walls, respectively. In particular, R/C nonstructural flat walls were implemented along the longitudinal direction as exterior/partition walls, as shown in Fig. 3 giving a typical exterior frame in the 10th story. The nonstructural walls were monolithically constructed with the beams, however, which were not considered in the structural design following the Japanese common practice. The nonstructural walls were reinforced with vertical and horizontal bars of #3, while additional bars of #5 were provided for vertical and diagonal bars reinforcing the wall edges and corners.

Fig. 1 – Northwest view of the investigated building

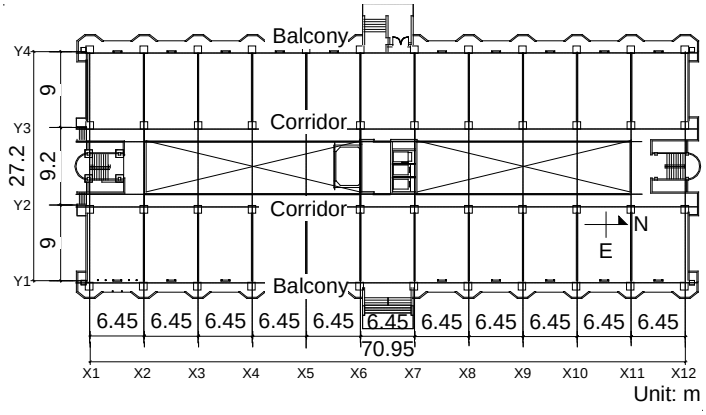

Fig. 2 – Ground floor plan of the investigated building

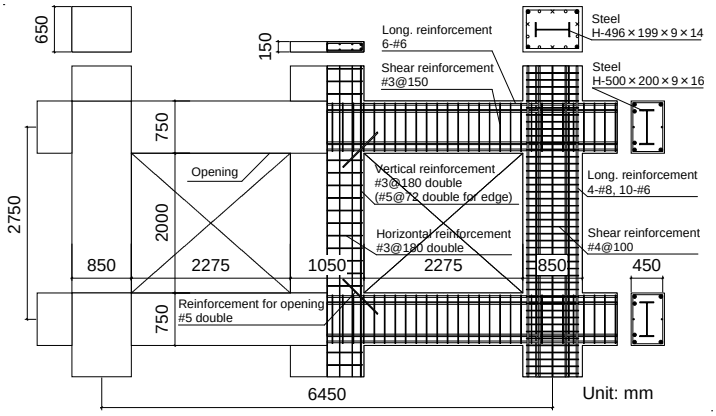

Fig. 3 – Typical exterior frame along the longitudinal direction

2.2 Summary of earthquake damage

The building suffered earthquake damage mainly along the longitudinal direction. Damage data on all components in the west tower (Y3 and Y4 frames) were collected through the authors' onsite inspection, as exemplified in Fig. 4, considering the symmetric plan of the building. Light damage was observed to the structural columns and beams, nevertheless, the nonstructural flat walls were severely damaged. The structural damage was mainly observed to the beam ends with the first-story column bottoms, as shown in Fig. 5; therefore, this building seemed to behave in a ductile manner during the earthquake. The maximum residual crack widths on the beams were approximately 1.0 mm, which indicated that the building could be recovered by typical schemes as cosmetic repair or epoxy injection in terms of the structural performance. In contrast, a large number of nonstructural walls needed to be replaced due to significant damage, as seen in Figs. 4 and 5. However, the effects of the nonstructural walls on the seismic performance of the building were quantitatively unclear.

Fig. 4 – Typical damage to the columns, beams, and nonstructural walls

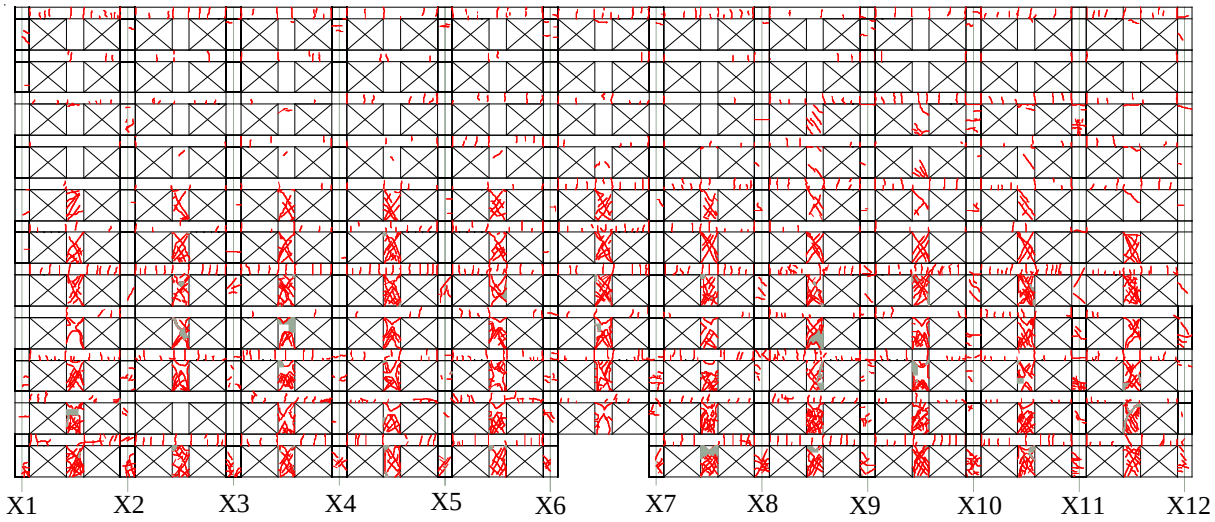

Fig. 5 – Damage to the Y4 frame

3. Experimental Program

3.1 Specimen

A laboratory test was conducted to investigate the effects of the typical nonstructural flat wall on the structural performance/behavior of the earthquake-damaged building mentioned above. Figure 6 presents a 1/2.5-scale model frame representing the typical one-bay in the 10th story of the building, as shown in Fig. 3. However, two biaxial load cells were inserted at the middle of the columns to experimentally obtain shear and axial forces induced on not only the columns but also the nonstructural wall. The columns were designed with the partial columns in the upper and lower stories to fix the specimen to a loading system, as described below. Table I summarizes the material properties of the specimen, respectively.

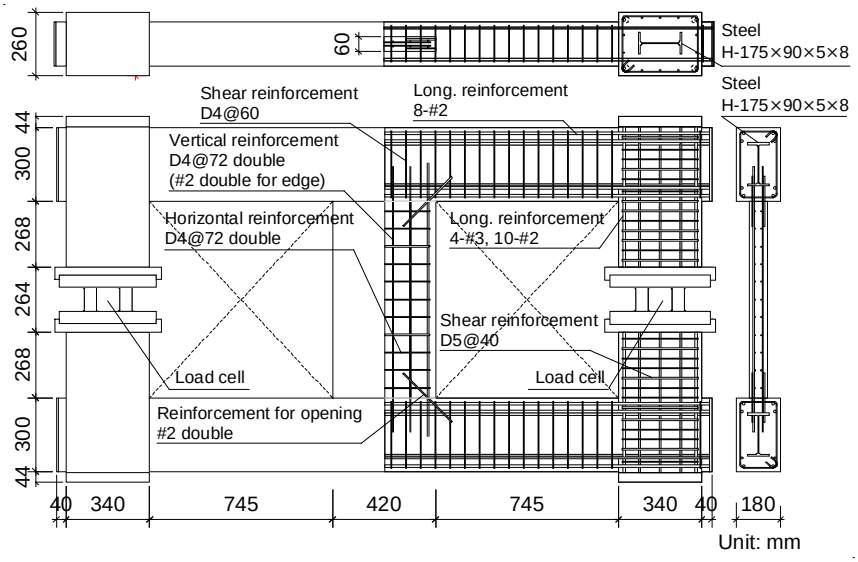

Fig. 6 – Structural drawing of the specimen

Table 1 – Material properties of the specimen

Concrete			
Design strength, F_c	Elastic modulus	Compressive strength	Tensile strength
21	2.30×10^4	28.6	2.28

Reinforcement			
Symbol	Elastic modulus	Yield stress	Tensile strength
D4	1.79×10^5	330	514
D5	1.54×10^5	352	529
#2	1.62×10^5	336	532
#3	1.72×10^5	359	531
SS400	1.86×10^5	300	557

Unit: N/mm^2

3.2 Experimental methods

Figure 7 shows a loading system for the test, on which the specimen was fixed to the basement and loading beam via four pin supports attached to the column tops and bottoms. The specimen was subjected to a constant axial load of 56 kN, equivalent to approximately 1.5% of the compressive strength of each column. This figure also shows static cyclic loads applied to the specimen in the horizontal direction, which were displacement-controlled by a lateral drift ratio defined as a ratio of the averaged inter-story drift (= $(\delta_2 + \delta_6 - \delta_3 - \delta_7)/2$ in the figure) to the story height of 1,100 mm. The loading beam above the specimen was maintained to be horizontal throughout the loading.

In this test, shear and axial forces applied to the columns were measured by the biaxial load cells installed at the middle of the columns, as shown in Figs. 6 and 7, to particularly clarify the performance/behavior of the nonstructural flat wall.

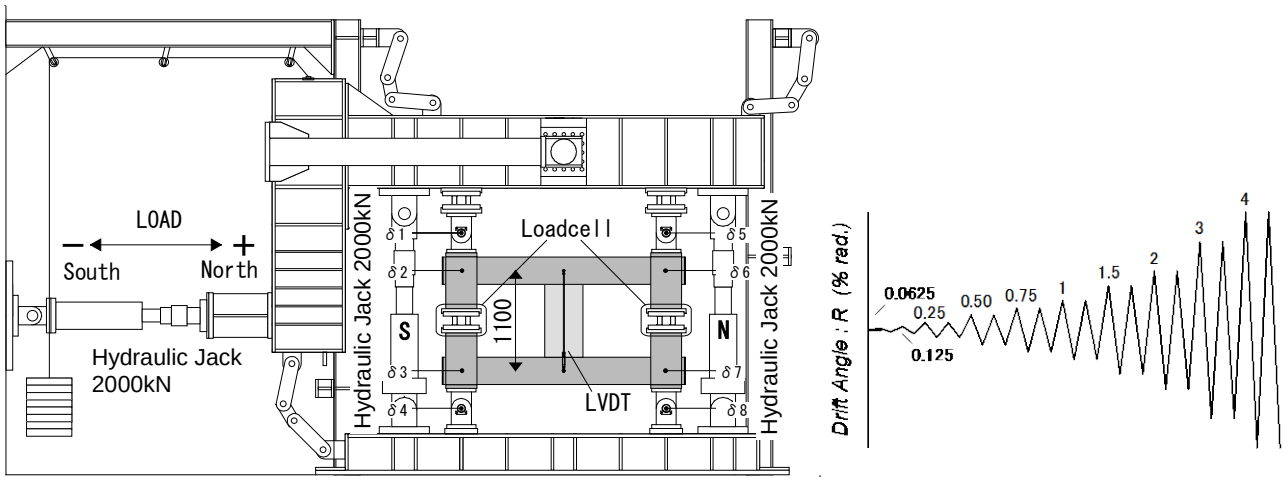

Fig. 7 – Loading scheme

4. Experimental Results

4.1 Overall behavior

Figures 8 and 9 present the shear force and lateral drift ratio relationship and the experimental damage development of the specimen. Flexural cracks initially occurred at the beam and wall ends during the first loading cycle. The vertical reinforcing bars in the nonstructural wall began to yield in the cycle to a 0.25% drift, which resulted in damage to the nonstructural wall exceeding a limitation for immediate occupancy, commonly defined as appearance of residual crack widths over 0.3 mm in Japan (Fig. 9(a)). The beams yielded in flexure in the cycle to a 0.75% drift. In the following cycle to a 1% drift, the nonstructural wall failed in shear (Fig. 9(b)); hence, the lateral strength of the specimen temporarily dropped, as shown in Fig. 8. A beam yielding mechanism was formed in the overall specimen with the shear failure of the wall. Spalling off of the concrete of the nonstructural wall was accelerated in the following cycle (Fig. 9(c)). The specimen finally deteriorated with buckling of beam longitudinal bars during the cycle to a 3% drift (Fig. 9(d)).

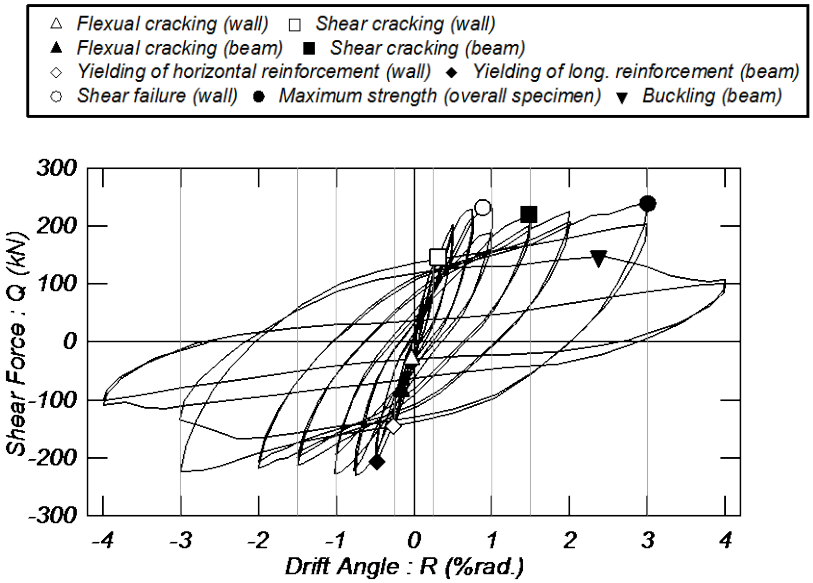

Fig. 8 – Story shear force vs. lateral drift ratio relationship of the specimen

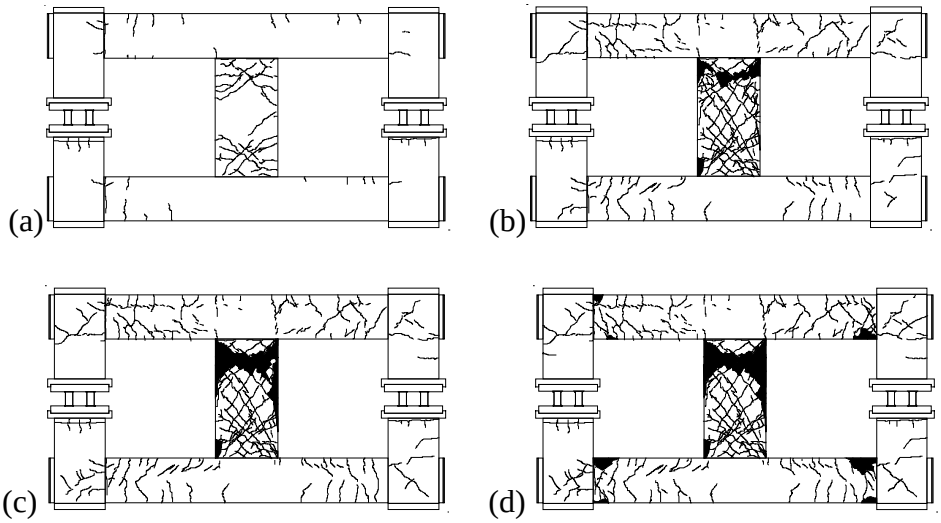

Fig. 9 – Damage development of the specimen: (a) 0.25% rad. (b) 1.0% rad. (c) 1.5% rad. (d) 3.0% rad.

4.2 Nonstructural wall behavior

Figure 10 focuses on the shear force of the nonstructural wall which was obtained by subtracting the column shear forces, which were measured by the load cells implemented into both columns, from the story shear force. The nonstructural wall sustained the maximum shear force of 87 kN at a 0.75% drift, which was approximately equivalent to 1/3 of the total shear force, as compared with Fig. 8. This result indicates that this type of nonstructural wall significantly contributes the structural performance until the shear failure. Therefore, a mechanism of inducing such high shear is investigated in the following.

Figure 11 shows the axial compression on the nonstructural wall observed at every peak drift during the cyclic loading. The axial compression increased up to ±0.75% drifts where the maximum lateral strengths were observed, as shown in Fig. 10. Such increases of the axial compression were caused because the upper and lower beams constrained the wall axial elongations which resulted from nonlinear characteristics of concrete, as illustrated in Fig. 12 comparing idealized elastic (Fig. 12(a)) and inelastic (Fig. 12(b)) strain profiles along the depth and height of a wall under an antisymmetric deformation. As shown in the figure, no axial elongation occurs under the elastic behavior maintaining a constant neutral axis depth at the middle of the wall depth over the wall height. In contrast, an axial elongation δ_a is caused by higher tensile strains across the wall depth excepting the inflection point at the middle height, due to shifting of the neutral axis depth to the wall edge in compression. The elongation δ_a is represented by an integration of the stains along the wall height at certain wall depth, as shown in the figure. As a result of constraint to the wall elongations by the beams, the increases of the axial compression occurred and resulted in increasing of the wall flexural strengths; hence, the relatively high lateral resistances were exhibited, as mentioned above.

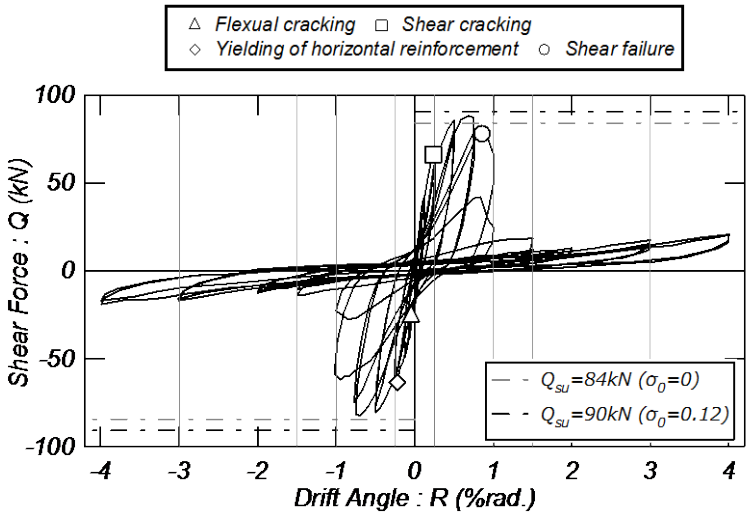

Fig. 10 – Shear force vs. lateral drift ratio relationship of the nonstructural wall

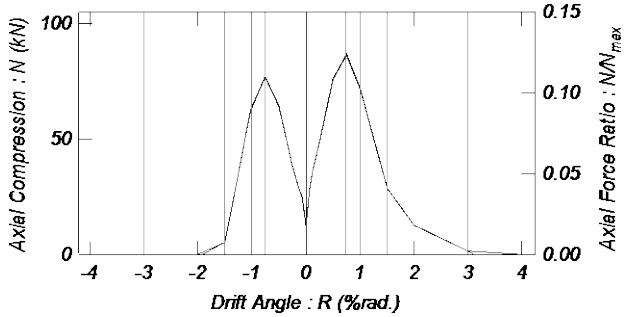

Fig. 11 – Axial compression of the nonstructural wall at the peak drifts

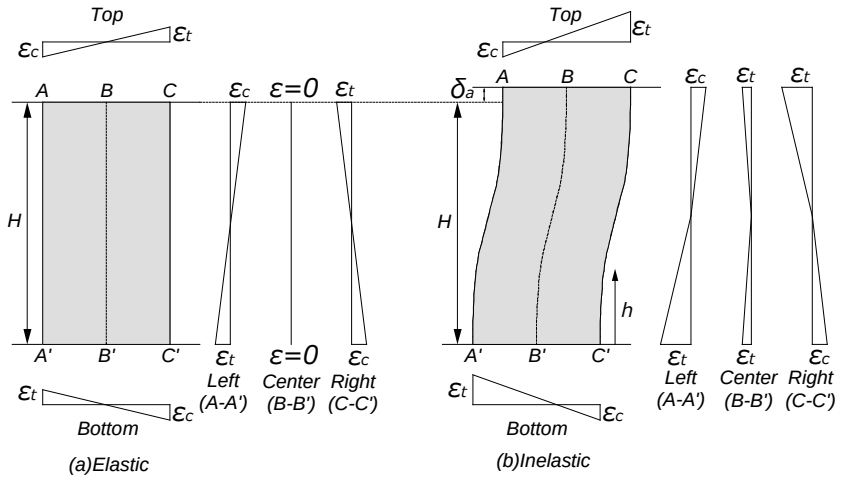

Fig. 12 – Mechanism of the wall axial elongation: (a) Elastic (b) Inelastic

5. Numerical Simulation of the Experiment

5.1 Modeling

Numerical simulations of the experiment were performed to particularly show appropriate modeling for the nonstructural flat wall.

Figure 13 shows an analytical model except for the nonstructural flat wall. The beams and columns were replaced by line elements with the MS models at both ends, to consider the axial-flexure interactions; however, rigid zones were provided from the pin supports at the column ends to the beam-column joints, as seen in the figure. The cross-sectional performance/behavior was represented by concrete and steel elements, as shown in Fig. 14. Concrete element was divided into ten layers considering core and cover concrete, steel shapes were divided into flanges and web with four layers, and reinforcing bars were placed according to the actual arrangement, as shown in the figure. The stress f_c-strain ε_c relationships of concrete was evaluated by the modified Kent and Park model [4], as shown in Fig. 15(a), in which the ascending curve was given by

$$f_c = Kf_c'\left[\frac{2\varepsilon_c}{0.002K} - \left(\frac{\varepsilon_c}{0.002K}\right)^2\right] \tag{1}$$

where K is a coefficient considers confining effects and f_c' is the uniaxial compressive strength of concrete (= F_c). The stress-strain relationships of steel was represented by a bilinear model considering the Bauschinger effect, as shown in Fig. 15(b).

The line elements considered stiffness degradations at shear cracking. The shear cracking strength Q_{cr} and drift R_{cr} were evaluated by Equations (2) and (3) according to the Japanese common practice. No columns/beams attained to the shear strengths in the following analyses.

$$Q_{cr} = \left(1+\frac{\sigma_0}{14.7}\right)\left[\frac{0.085k_c\left(F_c+49\right)}{M/\left(Qd\right)+1.7}\right]bj \tag{2}$$

$$R_{cr} = Q_{cr}/K_s \tag{3}$$

where σ_0 is the normal stress (in N/mm^2); k_c is a modification coefficient relating to the member depth (however, 1.0 for the specimen); M/Q is the shear span to depth ratio; d is the depth from the tensile reinforcing bars to the

compressive extreme fiber; b is the width; j is the distance between a compressive/tensile force couple on the critical section (commonly, replaced by (7/8)d); and K_s is the elastic shear stiffness.

The beams between the points A to C and D to F, where a nonstructural wall model was jointed as mentioned below, were assumed to be elastic for the axial behavior but rigid for bending and shear behavior.

The nonstructural flat wall was represented by the Isoparametric Element (IPE) model [5] in which the wall panel was replaced by a finite element, as shown in Fig. 16. The panel element can evaluate the axil-flexure-shear interactions under the two-dimensional stress field based on the material properties of concrete and reinforcing bars. The stress-strain behavior at the numerical integration points, whose number was assumed to be nine in this study, were evaluated based on the smeared crack model. The unconfined concrete model shown in Fig. 15(a) was applied in compression, however, considering a softening of the compressive strength under the two-dimensional stress field based on the Vecchio and Collins model [6] as

$$\frac{f_{c2\max}}{f_c'} = \frac{1}{0.8 - 0.34\varepsilon_1/\varepsilon_c'} \tag{4}$$

where f_{c2max} is a compressive strength of concrete reduced under the two-dimensional stress field; ε_1 is a principal tensile strain of concrete; and ε_c' is a strain at the compressive strength of concrete.

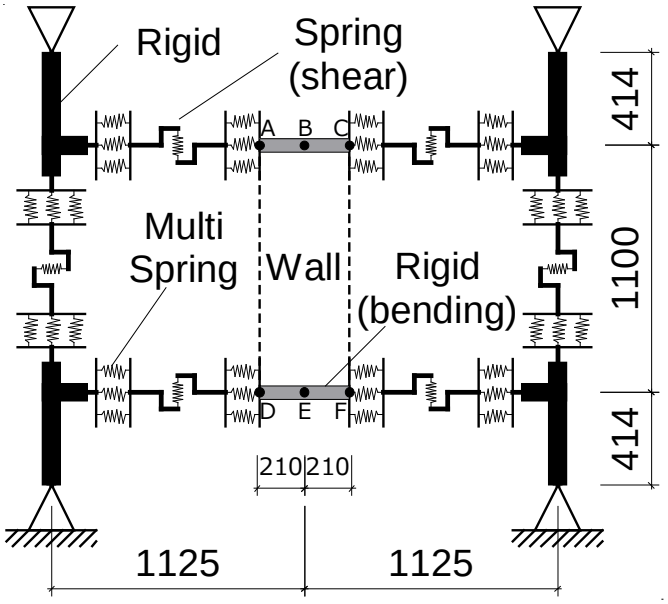

Fig. 13 – Modeling of the overall frame

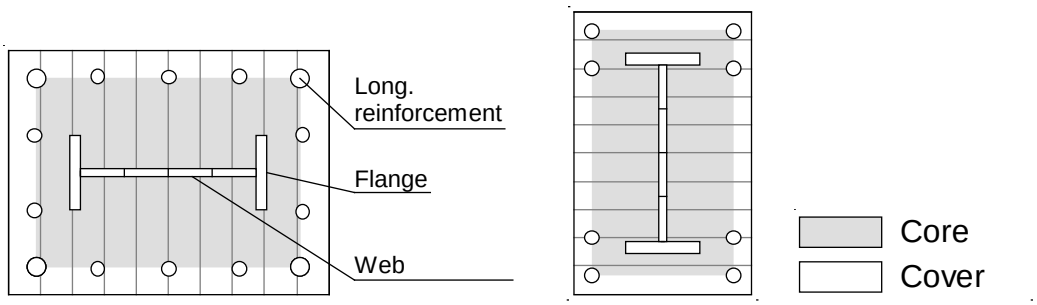

Fig. 14 – Modeling of the cross-sections of the columns (left) and beams (right)

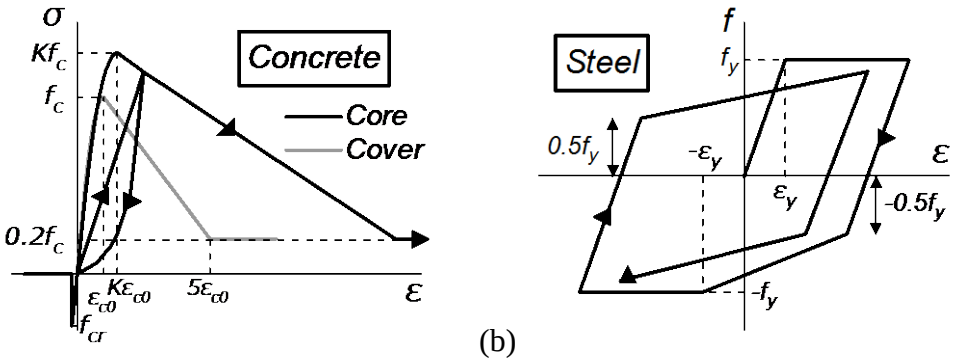

Fig. 15 – Material models for concrete and steel. (a) Modified Kent and Park model. (b) Bilinear model considered the Bauschinger effect

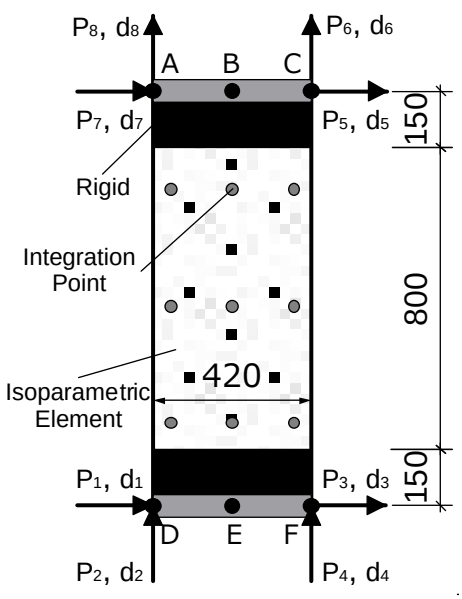

Fig. 16 – Modeling of the nonstructural wall

5.2 Simulation results

The analytical results are compared to the experimental ones in Figs. 17 to 19. Figure 17 compares the story shear force vs. lateral drift ratio relationships from the analysis with the experimental result up to a 3% drift, excluding the data after buckling of reinforcing bars was observed in the experiment, because the bar buckling was not addressed in the analyses. The analytical results well agreed with the test result. Figure 18 compares the shear force of the nonstructural flat wall vs. lateral drift ratio relationships between the analysis and the experiment in which the wall shear force was obtained as mentioned previously. The experimental nonstructural wall behavior including the deterioration after the shear failure could also be simulated by the IPE model, which indicate that the lateral performance/behavior of the nonstructural wall monolithically constructed in the moment-resisting frame can be evaluated by considering the axial-flexure-shear interactions. Moreover, the axial forces applied to the nonstructural wall in the analysis were compared with the experimental result, as shown in Fig. 19 presenting the axial force vs. lateral drift ratio relationships at every peak drift during the cyclic loading. The IPE model could simulate the loss of the axial resistance after the shear failure because of its consideration of the axial-flexure-shear interactions.

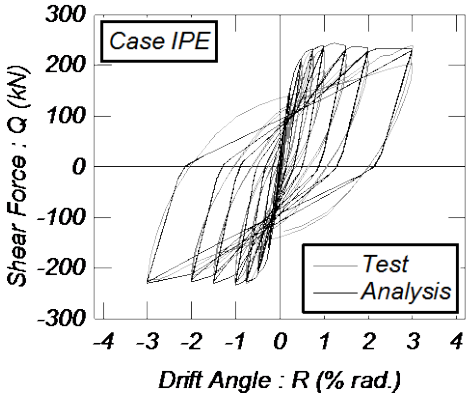

Fig. 17 – Comparisons of the story shear force vs. lateral drift ratio relationships

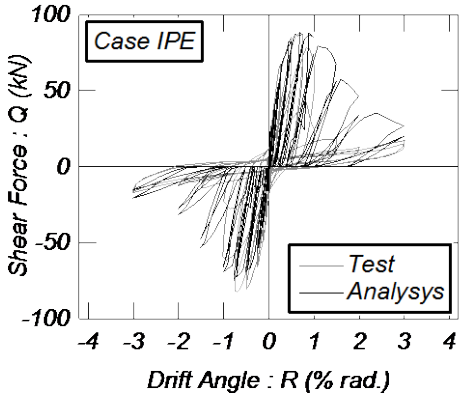

Fig. 18 – Comparisons of the wall shear force vs. lateral drift ratio relationships

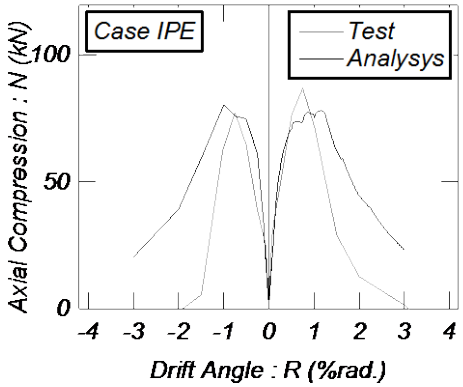

Fig. 19 – Comparisons of the wall axial force vs. lateral drift ratio relationships

6. Conclusions

The present paper investigated the effects of RC nonstructural flat walls on the seismic performance/behavior of typical middle-rise moment-resisting buildings in Japan because of a lack of knowledge in the previous studies. Major findings from the experimental and analytical studies are summarized as follows:

The experimental study successfully obtained the seismic behavior of the typical nonstructural wall in the 1-bay SRC moment-resisting frame. The nonstructural wall sustained more than 30% of the lateral force prior to

the shear failure, which resulted from the axial force of more than 10% of the compressive strength applied to the wall. The mechanism of the nonstructural wall-frame interactions was presented in the paper.

The IsoParametric Element (IPE) model simulated well the experimental behavior of the nonstructural wall considering the nonstructural wall-frame interactions. The axial-flexure-shear interactions must be taken into account for simulating the loss of axial resistance of the nonstructural wall involved in the shear failure.

7. Acknowledgements

This study was financially supported by JSPS KAKENHI Grant Number 25420578.

8. References

[1] AIJ (Architectural Institute of Japan) (2012): *Preliminary Reconnaissance Report of the 2011 Tohoku-Chiho Taiheiyo-Oki Earthquake*. Springer: Tokyo, Japan.

[2] AIJ (Architectural Institute of Japan) (1995): *Preliminary Reconnaissance Report of the 1995 Hyogoken-Nanbu Earthquake*. Architectural Institute of Japan: Tokyo, Japan.

[3] Nakano Y, Maeda M, Kuramoto H, Murakami M (2004): Guideline for Post-Earthquake Damage Evaluation and Rehabilitation of RC Buildings in Japan. *13th World Conference on Earthquake Engineering*, Vancouver, Canada, No. 124.

[4] Park R, Priestley MJN, Gill WD (1982): Ductility of Square-Confined Concrete Columns. *Journal of the Structural Division, ASCE*, **108**(4), 929-950.

[5] Chen S, Kabeyasawa T (2000): Modeling of Reinforced Concrete Shear Wall for Nonlinear Analysis. *12th World Conference on Earthquake Engineering*, Auckland, New Zealand, No. 1596.

[6] Vecchio FJ, Collins MP (1986): The Modified Compression-Field Theory for Reinforced Concrete Elements Subjected to Shear. *ACI Journal*, **83**(2), 219-231.